

Missing-Modality-Aware Graph Neural Network for Cancer Classification

Sina Tabakhi, *Member, IEEE*, and Haiping Lu, *Senior Member, IEEE*

Abstract—A key challenge in learning from multimodal biological data is missing modalities, where all data from some modalities are missing for some patients. Current fusion methods address this by excluding patients with missing modalities, imputing missing modalities, or making predictions directly with partial modalities. However, they often struggle with diverse missing-modality patterns and the exponential growth of the number of such patterns as the number of modalities increases. To address these limitations, we propose **MAGNET** (**M**issing-modality-**A**ware **G**raph neural **N**ETwork) for direct prediction with partial modalities, which introduces a *patient-modality multi-head attention* mechanism to fuse lower-dimensional modality embeddings based on their importance and missingness. **MAGNET**'s complexity increases linearly with the number of modalities while adapting to missing-pattern variability. To generate predictions, **MAGNET** further constructs a patient graph with fused multimodal embeddings as node features and the connectivity determined by the modality missingness, followed by a conventional graph neural network. Experiments on three public multiomics datasets for cancer classification, with *real-world instead of artificial missingness*, show that **MAGNET** outperforms the state-of-the-art fusion methods. The data and code are available at <https://github.com/SinaTabakhi/MAGNET>.

Index Terms—Multimodal learning, missing modalities, attention mechanism, graph neural network, cancer classification.

I. INTRODUCTION

CANCER development is a complex process driven by interactions across multiple molecular layers [1]–[3]. To unravel this complexity, cancer research increasingly profiles patients using these molecular modalities, known as multiomics. Each omics modality provides unique value individually while multimodal fusion can offer complementary insights [4], [5]. Multimodal machine learning approaches integrate these biological modalities to construct a comprehensive patient profile for improving downstream predictive tasks, such as cancer classification and subtyping [6]–[8].

Despite the effectiveness of multimodal biological data fusion, conventional approaches often assume that all omics modalities are available for each patient [9], [10]. However, missing modalities, characterized by structured missingness where all data from some modalities are missing for some patients, are an unavoidable challenge in biomedical applications [11]. For example, some patients may have missing transcriptomic profiles due to sample degradation or insufficient RNA quality, while others may lack proteomic data because of cost constraints or technical limitations [12], [13]. Therefore,

robust and effective multimodal fusion models are important for handling partial modalities.

There are three main approaches to handling missing modalities. The first approach excludes patients with missing modalities [10], [14], which can significantly reduce the number of available patients [15], [16] and introduce bias [5]. The second approach imputes missing modalities using simple methods like zero-filling [17] or advanced methods like statistical estimation [15] and deep generative models [18]. However, imputation may fail to distinguish genuinely missing modalities from zeros [17], introduce noise due to a limited number of patients [14], assume equal importance for all modalities [19], or rely on strong data distribution assumptions [20]. The third approach directly makes predictions with partial modalities [19], [21], addressing the limitations of the previous two approaches.

We adopt the third and most recent approach, where three less-explored challenges deserve attention:

- **Challenge 1: diverse missing-modality patterns.** Direct methods (the third approach) often assume that missingness occurs in a single modality [19], [22]. Furthermore, several methods only address missing modalities in the test data [23]–[25]. However, in healthcare, missing modalities can arise in various patterns and across both training and test data [16]. Fig. 1 shows an example of different missing-modality patterns in multimodal data.
- **Challenge 2: multimodal missingness scalability.** Several direct methods construct separate sub-models or mechanisms for each missing-modality pattern [19], [21]. While manageable for two modalities, this strategy struggles with more modalities due to the exponential growth of possible missing-pattern combinations, especially in healthcare applications [15], [26]. For M modalities, there are $2^M - 1$ missing patterns, making the scalability of multimodal missingness a significant challenge [15].
- **Challenge 3: real-world missingness evaluation.** A common practice for evaluating missing-modality handling methods involves artificially introducing missingness into otherwise complete datasets [27]. However, this evaluation approach can oversimplify or misrepresent *real-world missingness* patterns, particularly when complex, multivariate dependencies are ignored [11]. Moreover, it is susceptible to training-time bias, where knowledge about the missing modalities is unintentionally utilized during model training. As a result, this artificial-missingness evaluation approach may fail to reflect real-world missingness challenges.

Sina Tabakhi and Haiping Lu are with the Centre for Machine Intelligence and the School of Computer Science, University of Sheffield, S1 4DP, Sheffield, U.K. (e-mail: stabakhi1@sheffield.ac.uk; h.lu@sheffield.ac.uk).

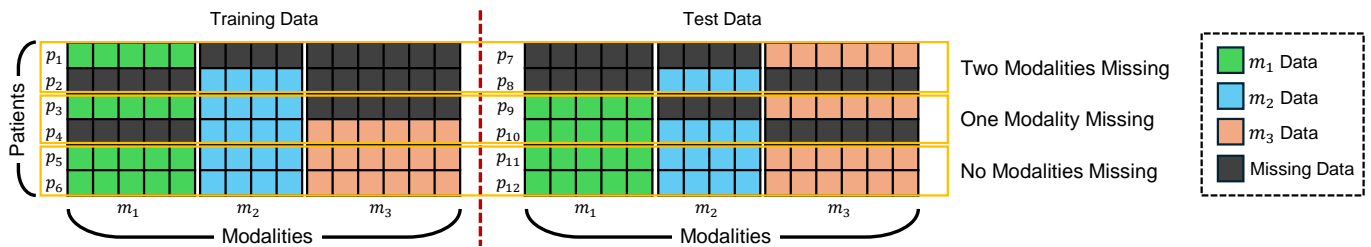


Fig. 1. Different missing-modality patterns (zero, one, or two modalities missing) across 12 patients with three modalities. Each colored row within a modality shows a patient’s respective data, while a gray row indicates a missing modality for that patient. Moreover, both training and test data can have missing modalities. With three modalities, each patient’s data can have $2^3 - 1 = 7$ possible missing patterns.

To address these challenges, we propose MAGNET (Missing-modality-Aware Graph neural NETWORK) for direct prediction with partial omics modalities, with two key contributions:

- 1) To tackle challenges 1 and 2, MAGNET encodes each modality into lower-dimensional representations of the same size and then introduces a *patient-modality multi-head attention* (PMMHA) mechanism to fuse these representations into a shared multimodal representation. This mechanism handles diverse missing-modality patterns using a *binary modality mask*, which zeros out the attention weights of missing modalities, ensuring that only available modalities contribute to the fused representation. Moreover, MAGNET linearly manages the increase in the number of modalities because adding one new modality requires only one additional encoder to learn its representation and an expansion of the attention weights with one extra column for the new modality. This design keeps the model simple and expandable. To ensure that the fused representation preserves patient-level structure from the input space, we introduce a *Kullback–Leibler (KL) divergence-based loss* that aligns patient similarity distributions before and after fusion. This allows us to preserve relationships among patients even in the presence of missing modalities. After generating multimodal embeddings, MAGNET constructs a *patient interaction graph* that leverages modality missingness for edge connectivity and fused representations as node features, capturing holistic structures. A graph neural network (GNN) learns patient representations from this graph to generate final predictions.
- 2) To address challenge 3, we evaluate MAGNET on multi-omics datasets for cancer classification with real-world rather than artificial missingness. The results demonstrate that MAGNET consistently outperforms state-of-the-art fusion methods across multiple evaluation metrics.

A key benefit of MAGNET is its alignment with real-world clinical practice. Doctors often make decisions by analyzing patient relationships, as those similar in one modality are likely to share characteristics in other, potentially missing, modalities [15]. MAGNET resonates with this approach through the patient interaction graph, where edges connect patients sharing at least one common modality, enabling the model to leverage missing modality information more effectively.

II. RELATED WORK

A. Multimodal Learning for Cancer

Advancements in sequencing technologies have enabled the simultaneous profiling of multiple biological data, termed multiomics [4], [28], driving the development of fusion methods in cancer research [29]–[31]. SNF [9] employs a message-passing approach to iteratively combine patient similarity networks from each omic. INF [32] extends SNF by integrating multiomics data with a feature-ranking mechanism. EMOGI [33] introduces an explainable graph convolutional network (GCN) to identify cancer genes through multiomics integration. TREE [3] proposes a transformer-based model with graph representation learning to integrate multiomics data. MOGONET [10] is a late-fusion framework built using supervised GCN. These methods assume all modalities are available for each patient, limiting their ability to handle missing modalities. Missing modalities are a common challenge in healthcare, caused by low tissue quality, insufficient sample volume, measurement limitations, cost constraints, or patient dropout [11], [34].

B. Multimodal Learning with Missing Modalities

The main focus of this paper is on handling missing modalities, and addressing missing values is beyond its scope. Multimodal models for addressing missing modalities categorize into three approaches. The simplest approach considers only patients with all modalities available, applying methods designed for complete datasets [9], [10], [35]. While straightforward, this significantly reduces the number of patients and ignores valuable information from those with missing modalities, particularly in healthcare where patients with complete modalities are limited [14], [36].

Imputation offers an alternative by filling or reconstructing missing modalities using various strategies. One strategy concatenates all modalities, treating missing modalities as missing data at random and estimating them based on existing values [37]–[39]. However, this ignores the natural correlation of features within the same modality [11], [15]. Another strategy uses statistical methods that account for the structure of missing modalities. TOBMI [40] applies a weighted k NN method to impute block-wise missing multiomics. M3Care [15] imputes missing modalities in latent space by identifying similar patients and concatenates the imputed representations to perform clinical tasks. Deep generative models provide another imputation strategy by reconstructing missing modalities

TABLE I
NOTATIONS AND DESCRIPTIONS

Notation	Description
$\mathbf{a}^m \in \mathbb{R}^{N \times 1}$	Attention weights for modality m from \mathbf{A}
$\mathbf{A} \in \mathbb{R}^{N \times M}$	Attention coefficient matrix in the PMMHA
β	Edge discard threshold in graph \mathcal{G}
d_h	Embedding size for each head in the PMMHA
$\mathcal{D} = \{\mathbf{X}^1, \dots, \mathbf{X}^M\}$	Multimomics dataset with M modalities
\mathbf{e}_{uv}	Edge feature between nodes u and v in graph \mathcal{G}
$\mathcal{G} = (\mathcal{V}, \mathcal{E})$	Patient graph with nodes \mathcal{V} and edges \mathcal{E}
$\mathcal{H} \in \mathbb{R}^{N \times M \times d}$	Stacked representations across modalities
$\mathbf{H}^i \in \mathbb{R}^{N \times d}$	i th modality representation of dimension d
K	Number of heads in the PMMHA
L	Number of layers in the GNN
λ	KL divergence loss coefficient
$\mathbf{M} \in \{0, 1\}^{N \times M}$	Binary modality mask matrix
M	Number of omics modalities
$\mathcal{N}(u)$	Neighbors of node u in graph \mathcal{G}
N	Number of patients
$\mathbf{X}^i \in \mathbb{R}^{N \times d_i}$	i th omics data with N patients and d_i features
$\mathbf{y}, \hat{\mathbf{y}} \in \mathbb{R}^N$	True and predicted labels for N patients
$\mathbf{z}_u^{(l)}$	Embedding of node u at the l th layer of GNN
$\mathbf{Z} \in \mathbb{R}^{N \times d}$	Fused embeddings for all patients

from available ones. Common models include autoencoders [18], [41], [42], generative adversarial networks [43], [44], and diffusion models [45]. These models may treat modalities as similar [19], introduce imputation noise [14], [15], or rely on strong data distribution assumptions [16].

Direct prediction is another approach that incorporates specialized designs to perform downstream tasks with missing modalities. NEMO [46] manages missing modalities using a neighborhood-based approach with average similarities. MRGCN [47] uses a GCN-based encoder-decoder method with an indicator matrix to address missing modalities. GRAPE [20] and MUSE [16] leverage bipartite graphs with modalities and patients as nodes to directly address missing modalities. DrFuse [19] combines modality-specific and shared sub-models. MT [21] addresses cases where a specific modality is entirely missing in test data. ASR [48] is a sparse representation-based method that learns modality-specific sparse representations from available data and fuses them into a unified similarity matrix in an unsupervised setting. However, these methods may oversimplify relationships, struggle with multimodal missingness scalability due to exponentially growing missing patterns, or address only specific missing scenarios [15], [16].

III. METHODOLOGY

A. Notation

The common notations used in the paper are listed in Table I. We use bold lowercase letters for vectors, bold uppercase letters for matrices, and calligraphic letters for sets throughout the paper.

B. Problem Formulation

Definition 1 (Supervised Multimodal Omics Learning): In the context of multimomics, supervised multimodal learning involves leveraging multiple biological data to build predictive models. Formally, let $\mathcal{D} = \{\mathbf{X}^1, \mathbf{X}^2, \dots, \mathbf{X}^M\}$ represent the

M omics modalities, where $\mathbf{X}^i \in \mathbb{R}^{N \times d_i}$ denotes the i th omics modality with N patients and d_i features. Given the corresponding labels $\mathbf{y} \in \mathbb{R}^N$ (e.g., cancer subtypes), the classification task is to learn a mapping $f_\theta : \mathcal{D} \rightarrow \mathbf{y}$ that minimizes the loss function $\mathcal{L}(\mathbf{y}, \hat{\mathbf{y}})$, where $\hat{\mathbf{y}} = f_\theta(\mathcal{D})$ represents the predicted labels. Here, θ is the set of learnable parameters of the predictive model f_θ , which are optimized during training to minimize the loss \mathcal{L} .

Definition 2 (Multimomics with Missing Modalities): In real-world multimomics datasets, some modalities may be missing for some patients, impacting the integration of multiple omics modalities. Formally, let $\mathbf{M} \in \{0, 1\}^{N \times M}$ be a binary modality mask matrix, where $\mathbf{M}_{ji} = 1$ indicates that the i th modality is available for the j th patient, and $\mathbf{M}_{ji} = 0$ indicates its absence. For omics modality data i , \mathbf{X}^i , the j th patient’s data is considered if $\mathbf{M}_{ji} = 1$. The problem is to construct a model f that can robustly handle missing modalities in \mathcal{D} while still learning the relationships across available modalities.

C. The MAGNET Framework

Fig. 2 illustrates the overall architecture of MAGNET, which consists of three modules. The first module, “*Modality-Specific Encoder*”, encodes each omics-specific modality into a lower-dimensional representation. The second module, “*Patient-Modality Multi-Head Attention Integration*”, assigns different weights to each modality for each patient using a binary modality mask and fuses all patient embeddings across modalities into a single unified embedding. The third module, “*Patient Graph Construction and GNN Classification*”, constructs a graph to represent interactions between patients while accounting for missing modalities. Then, a GNN classifier learns from this constructed graph to make the final prediction. Each module, along with the training strategy, is detailed in the following sections. Furthermore, we discuss the key strengths of MAGNET.

D. Modality-Specific Encoder

Since each omics modality consists of high-dimensional data with varying dimensionalities, we first transform each modality into a lower-dimensional embedding of the same size using multi-layer perceptron (MLP) encoders. Specifically, for modality i , the corresponding embedding space is constructed as follows:

$$\mathbf{H}^i = \text{MLP}^i(\mathbf{X}^i; \mathbf{W}_{\text{MLP}}^i), \quad (1)$$

where $\mathbf{H}^i \in \mathbb{R}^{N \times d}$ is the resulting embedding with a fixed dimensionality d , MLP^i represents the MLP encoder for modality i , and $\mathbf{W}_{\text{MLP}}^i$ represents the learnable parameter of the encoder. This ensures that all modalities are projected into the same size embedding space, facilitating subsequent integration and learning tasks.

E. Patient-Modality Multi-Head Attention Integration

To address missing modalities and enable the integration of patient embeddings across available modalities, we introduce a PMMHA mechanism. This mechanism calculates attention weights for each modality specific to each patient, enabling

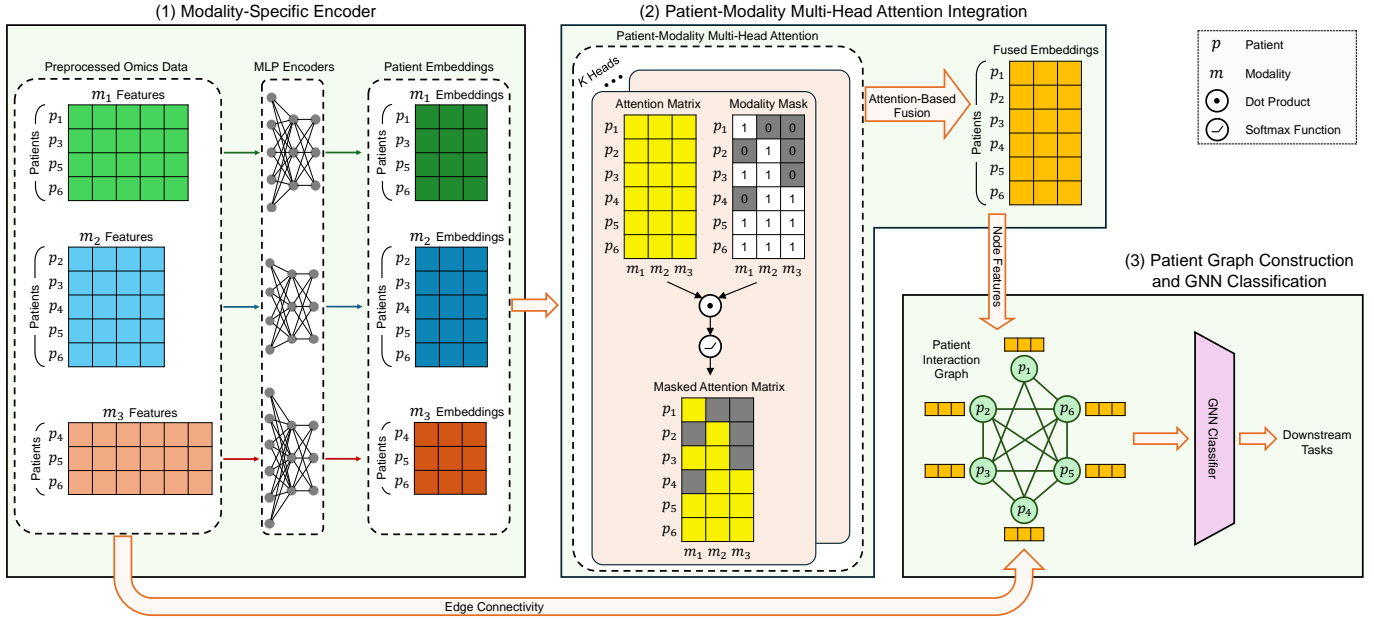


Fig. 2. MAGNET performs classification tasks in three steps. (1) MAGNET encodes each modality into a lower-dimensional embedding of the same size. (2) A patient-modality multi-head attention mechanism computes the importance of each modality for each patient and applies a modality mask to set attention weights to zero for missing modalities. It aggregates patient embeddings into a fused embedding using the attention weights. (3) MAGNET constructs a patient interaction graph, where nodes represent patients with fused embedding as features, and edges connect patients sharing at least one available modality. Finally, a GNN learns from this graph to perform downstream tasks.

selective weighting of modality contributions based on their importance.

In a patient-modality single-head attention (PMSHA) mechanism, the modality-specific embeddings are first stacked to form the tensor $\mathcal{H} \in \mathbb{R}^{N \times M \times d}$. A linear transformation is then applied to transform this tensor into higher-level features using a learnable weight matrix $\mathbf{W}_{\text{lin}} \in \mathbb{R}^{d \times d}$.

Next, an attention coefficient matrix is calculated to evaluate the importance of each modality for each patient, incorporating the binary modality mask \mathbf{M} . To ensure the coefficients are comparable across modalities, they are normalized using the softmax function. This process is defined as:

$$\mathbf{A} = \text{softmax}(\text{Linear}(\mathcal{H}; \mathbf{w}_{\text{att}}) \odot \mathbf{M}), \quad (2)$$

where $\mathbf{A} \in \mathbb{R}^{N \times M}$ represents the attention coefficient matrix, \mathbf{w}_{att} is a learnable parameter, and \odot is the dot (Hadamard) product. \mathbf{M} ensures that the attention weights for missing modalities are set to zero for each patient. Finally, the embeddings for each patient are fused using a weighted sum, where the attention coefficients determine the contribution of each modality. This is performed as:

$$\mathbf{Z} = \sum_{m=1}^M \mathbf{a}^m \odot \mathbf{H}^m, \quad (3)$$

where $\mathbf{Z} \in \mathbb{R}^{N \times d}$ is the fused embedding for all patients, and $\mathbf{a}^m \in \mathbb{R}^{N \times 1}$ is the attention weights for modality m extracted from \mathbf{A} .

To enhance the model's ability to capture diverse patterns in the data, PMMHA allows each head to focus on different aspects of the modality. Therefore, building on PMSHA, the transformed embedding \mathcal{H} is divided across K heads, where

K is the number of attention heads. The attention process is then applied independently to each head. Specifically, the embedding dimension for each head is $d_h = d/K$, and \mathcal{H} is reshaped into $\mathbb{R}^{N \times M \times d_h \times K}$. The normalized attention coefficients for each head k are then calculated as \mathbf{A}^k , and the embeddings for each head are fused separately based on these coefficients as \mathbf{Z}^k . Finally, the fused embeddings from all heads are concatenated and projected back into the input embedding space as:

$$\mathbf{Z} = \text{Concat}(\mathbf{Z}^1, \mathbf{Z}^2, \dots, \mathbf{Z}^K) \mathbf{W}_{\text{out}}, \quad (4)$$

where $\mathbf{W}_{\text{out}} \in \mathbb{R}^{d \times d}$ is a learnable weight matrix, and $\mathbf{Z} \in \mathbb{R}^{N \times d}$ represents the final fused embedding for all patients.

F. Patient Graph Construction and GNN Classification

With the fused embeddings generated for patients, we aim to make predictions by leveraging both relationships from the input multiomics data and holistic patterns captured in the fused embeddings.

MAGNET constructs a patient interaction graph $\mathcal{G} = (\mathcal{V}, \mathcal{E})$, where \mathcal{V} represents a set of N nodes corresponding to patients, and $\mathcal{E} \in \mathcal{V} \times \mathcal{V}$ represents edges connecting patients. Edges are formed using the binary modality mask \mathbf{M} , where an edge exists between two patients if they share at least one available modality. The fused embeddings serve as the initial node features of the graph. Moreover, we assign the cosine similarity between patients as the edge feature, computed from the input multiomics data based only on shared modalities. To ensure the graph focuses on the most relevant patient correlations, we retain only edges whose cosine similarity exceeds a specified threshold β . For nodes without any edge

after thresholding, we connect them to their most similar neighbor to preserve graph connectivity.

Given the constructed graph \mathcal{G} , MAGNET employs a multi-layer GNN, utilizing the graph sample and aggregation (GraphSAGE) operator [49], to encode the graph. At each layer, the GNN updates a patient's representation by aggregating feature information from its neighbors, allowing the model to incorporate local structural context and capture relationships between patients. This design also enables generating embeddings for unseen patients, as long as their neighborhood information is available [49], [50]. The GNN stacks multiple GraphSAGE layers, with each layer l defined as:

$$\mathbf{z}_u^{(l+1)} = \sigma \left(\mathbf{W}_{\text{root}}^{(l)} \cdot \mathbf{z}_u^{(l)} + \mathbf{W}_{\text{agg}}^{(l)} \cdot \mathbf{m}_u^{(l)} \right), \quad (5)$$

where

$$\mathbf{m}_u^{(l)} = \text{Mean} \left(\left\{ \mathbf{W}_{\text{msg}}^{(l)} \cdot [\mathbf{z}_v^{(l)} \parallel \mathbf{e}_{uv}] \mid v \in \mathcal{N}(u) \right\} \right), \quad (6)$$

$\mathbf{z}_u^{(l)}$ and $\mathbf{z}_v^{(l)}$ are rows of $\mathbf{Z}^{(l)}$, representing the embeddings of nodes u and v , respectively, \mathbf{e}_{uv} is the edge feature between nodes u and v , and $\mathbf{W}_{\text{root}}^{(l)}$, $\mathbf{W}_{\text{agg}}^{(l)}$, and $\mathbf{W}_{\text{msg}}^{(l)}$ are learnable weight matrices. In Equations (5) and (6), $\sigma(\cdot)$ represents the ReLU activation function, $\mathcal{N}(u)$ is the directly connected neighbors of node u , and \parallel is the concatenation operation. The initial node representations are the fused embeddings learned from the previous module, given by $\mathbf{Z}^{(0)} = \mathbf{Z}$.

Finally, we use the embedding generated at the last layer L , $\mathbf{Z}^{(L)}$, as input to an MLP decoder to produce the final predictions, defined as $\hat{\mathbf{y}} = \text{MLP}(\mathbf{Z}^{(L)}; \mathbf{W}_{\text{MLP}})$.

G. Learning Objective

We optimize the model parameters via backpropagation by minimizing a combined loss that balances prediction accuracy and representation quality. The first component is a *supervised cross-entropy loss*, which encourages the model to correctly classify each patient based on their graph-informed fused embedding. The second component is a *KL divergence-based loss* designed to preserve the structure of patient relationships during fusion. Specifically, it ensures that similarities between patients in the fused embedding space remain consistent with those computed from the input data, despite missing modalities. This encourages the model to maintain meaningful relational information while learning from partially observed data. The supervised cross-entropy loss is defined as:

$$\mathcal{L}_{\text{CE}}(\mathbf{y}, \hat{\mathbf{y}}) = \sum_{p=1}^N \text{CE}(y_p, \hat{y}_p), \quad (7)$$

where $\text{CE}(\cdot, \cdot)$ is the cross-entropy loss function between true label y_p and predicted label \hat{y}_p for patient p . To preserve patient-level similarity structure in the fused embedding space, we use a KL divergence-based loss:

$$\mathcal{L}_{\text{KL}} = \text{KL}(\mathbf{P} \parallel \mathbf{Q}) = \sum_{i=1}^N \sum_{\substack{j=1 \\ j \neq i}}^N P_{ij} \log \frac{P_{ij}}{Q_{ij}}, \quad (8)$$

where \mathbf{P} is the normalized cosine similarity matrix computed in the input space, and \mathbf{Q} is the normalized similarity matrix in the fused embedding space. Each element Q_{ij} is computed using a Student- t kernel [51] as:

$$Q_{ij} = \frac{(1 + \|\mathbf{z}_i - \mathbf{z}_j\|^2)^{-1}}{\sum_{k \neq l} (1 + \|\mathbf{z}_k - \mathbf{z}_l\|^2)^{-1}}, \quad (9)$$

where $\|\cdot\|^2$ denotes the squared Euclidean distance between the fused embeddings of two patients. The total loss is defined as:

$$\mathcal{L} = \mathcal{L}_{\text{CE}} + \lambda \cdot \mathcal{L}_{\text{KL}}, \quad (10)$$

where λ is a balancing coefficient.

H. Training Process

We train MAGNET using an inductive learning approach, ensuring that patients in the test set are not utilized during the training phase. When constructing the patient graph, all edges connecting patients in the training set to those in the test set are excluded. Moreover, loss computation is performed exclusively on the patients in the training set. A detailed description of MAGNET is provided in Algorithm 1.

Algorithm 1 The MAGNET Algorithm

Input

- \mathcal{D} : training multiomics dataset
- \mathbf{M} : binary modality mask

Output

- $\hat{\mathbf{y}} \in \mathbb{R}^N$: predicted labels

- 1: Construct patient graph \mathcal{G} with edges formed using \mathbf{M}
 - 2: Set edge feature in \mathcal{G} from patient similarity in \mathcal{D}
 - 3: **for** $t = 1$ **to** T **do**
 - 4: **for** $m = 1$ **to** M **do**
 - 5: Encode modality m using Eq. (1)
 - 6: **end for**
 - 7: Compute attention \mathbf{A} for each head using Eq. (2)
 - 8: Fuse patient embeddings to obtain \mathbf{Z} using Eq. (4)
 - 9: Initialize graph node features in \mathcal{G} with \mathbf{Z}
 - 10: Apply GNN to \mathcal{G} to learn embeddings via Eq. (5)
 - 11: Predict labels $\hat{\mathbf{y}}$ using the MLP decoder
 - 12: Compute the cross-entropy loss using Eq. (7)
 - 13: Compute the KL divergence loss using Eq. (8)
 - 14: Update model parameters using the total loss in Eq. (10)
 - 15: **end for**
-

I. Discussion

1) *Robustness to Missing Modalities*: Conventional fusion methods often aggregate embeddings across modalities without considering their varying importance. In contrast, MAGNET introduces PMMHA to calculate modality importance for each patient, enabling weighted aggregation of available modalities. To handle diverse missing-modality patterns, we introduce a binary modality mask matrix \mathbf{M} , which zeros out attention weights for missing modalities. For example, if only one modality is available for a patient, its attention weight becomes

TABLE II
SUMMARY OF MULTIOMICS DATA CHARACTERISTICS.

Dataset	#Patients	Classes	#Patients in Omics (Missing Rate %)			#Selected Features		
			DNA	mRNA	miRNA	DNA	mRNA	miRNA
BRCA	956	Luminal A: 434, Luminal B: 194, Basal-like: 142, Normal-like: 119, HER2-enriched: 67	328 (65.69)	956 (00.00)	584 (38.91)	1,000	1,000	436
BLCA	433	High-grade: 412, Low-grade: 21	431 (00.46)	423 (02.31)	426 (01.62)	1,000	1,000	471
OV	360	Short-term survivors: 184, Long-term survivors: 176	356 (01.11)	184 (48.89)	302 (16.11)	1,000	1,000	448

one, and its embedding is used. Similarly, if two modalities are available, attention weights are computed for those, and their embeddings are fused accordingly. Even when no modalities are missing, MAGNET performs effectively. This design ensures robust handling of missing-modality patterns in training and testing data.

2) *Linear Complexity with Modality Growth*: MAGNET maps each modality to a lower-dimensional space and generates fused multimodal embeddings through the introduced PMMHA mechanism. Adding a new modality requires only an additional encoder for its embeddings and extending \mathbf{A} with one additional column to represent its importance for each patient. Once fused multimodal embeddings are obtained, GNN operates independently of the number of modalities, relying on the number of patients. Thus, the model achieves linear complexity with respect to M modalities, $\mathcal{O}(M)$, making it efficient for multimodal learning. Details of the experimental execution time analysis are provided in the Supplementary Material (Appendix D).

IV. EXPERIMENTS

A. Experimental Settings

1) *Datasets and Preprocessing*: To evaluate MAGNET, we use three publicly available multiomics datasets from The Cancer Genome Atlas [52], obtained via the UCSC Xena tool,¹ which present real-world missingness at varying rates:

- Breast invasive carcinoma (BRCA): This dataset uses the PAM50 classifier, a 50-gene signature, to categorize BRCA into five subtypes based on gene expression: Luminal A, Luminal B, basal-like, HER2-enriched (HER2), and normal-like [53].
- Bladder urothelial carcinoma (BLCA): This dataset includes bladder cancer cases, classified as low-grade or high-grade for grade classification [54].
- Ovarian serous cystadenocarcinoma (OV): This dataset contains ovarian cancer samples, divided into long-term (survival time ≥ 3 years) and short-term (survival time < 3 years with 'DECEASED' status) survivors [55].

We analyze three omics modalities across all datasets: DNA methylation (DNA), gene expression RNAseq (mRNA), and miRNA mature strand expression RNAseq (miRNA). For the DNA modality, we use the Illumina Infinium HumanMethylation27 for BRCA and OV, and the HumanMethylation450 for BLCA. The mRNA modality uses the Illumina HiSeq pancan normalized version, and the miRNA modality includes Illumina HiSeq data. Further details are available on the UCSC Xena platform [56].

¹<https://xenabrowser.net/datapages/>

To prepare datasets for analysis, we preprocess each omics modality separately. First, we remove features with more than 10% missing values and fill the remaining missing values using the feature-wise mean. Second, we normalize each feature to the $[0, 1]$ range using min-max scaling [20]. Third, we exclude low-variance features with limited discriminatory ability, applying modality-specific thresholds: 0.04 for DNA in BRCA and OV, 0.08 for DNA in BLCA, and 0.03 for mRNA across all datasets. No variance filtering is applied to miRNA due to its smaller number of features. Given the high dimensionality of each omics modality, we further reduce irrelevant and redundant features using the ANOVA [57] feature selection method implemented in scikit-learn. For DNA and mRNA, we retain the top 1,000 selected features, while no feature selection is applied to miRNA due to its limited number of features. Table II presents an overview of the dataset statistics.

2) *Evaluation Metrics*: We evaluate the performance of fusion methods on the BLCA and OV datasets for binary classification using accuracy, area under the precision-recall curve (AUPRC), area under the receiver operating characteristic curve (AUROC), and Matthews correlation coefficient (MCC). For multi-class classification on the BRCA dataset, we assess performance using accuracy, macro-averaged F1 score (Macro F1), weighted-averaged F1 score (Weighted F1), and MCC.

3) *Evaluation Strategies*: To evaluate classification performance, we divide each dataset into matched data (patients with all modalities available) and unmatched data (patients with missing modalities). Each subset is further split into training, validation, and test sets with a ratio of 7:1:2, ensuring diverse missing patterns in training and test data. Matched and unmatched subsets are then combined to form the final training, validation, and test sets. For hyperparameter tuning, models are trained on the training set, and the best parameters are selected by monitoring performance on the validation set. Due to the limited sample size, the training and validation sets are combined after hyperparameter tuning to form the final training set. All methods are trained on this combined training set, and performance metrics are evaluated on the test set. To ensure robustness, all evaluations are performed five times, with results reported as the mean and standard deviation of the metrics. For consistency, the same data splits are used across all methods.

4) *Implementation Details*: We implement MAGNET in Python 3.10 using PyTorch 2.1.0 and PyTorch Geometric 2.4.0. The Adam optimizer [58] is used for training, with a step decay learning rate scheduler that reduces the learning rate by a factor of 0.8 every 20 epochs. All models are

TABLE III
CLASSIFICATION PERFORMANCE COMPARISON ON THE BRCA, BLCA, AND OV DATASETS, REPORTED AS THE MEAN \pm STANDARD DEVIATION OVER FIVE INDEPENDENT RUNS (**BEST**, **SECOND-BEST**).

Dataset	Metric	MOGONET-Zero [10]	MOGONET- k NN [10]	MRGCN [47]	M3Care [15]	MUSE [16]	MAGNET
BRCA	Accuracy (\uparrow)	0.795 \pm 0.025	0.847 \pm 0.015	0.844 \pm 0.009	0.899 \pm 0.016	0.895 \pm 0.021	0.918\pm0.012
	Macro F1 (\uparrow)	0.638 \pm 0.062	0.794 \pm 0.035	0.826 \pm 0.014	0.872 \pm 0.018	0.880 \pm 0.014	0.902\pm0.019
	Weighted F1 (\uparrow)	0.758 \pm 0.036	0.838 \pm 0.018	0.842 \pm 0.008	0.898 \pm 0.015	0.894 \pm 0.022	0.917\pm0.011
	MCC (\uparrow)	0.706 \pm 0.035	0.781 \pm 0.022	0.778 \pm 0.012	0.858 \pm 0.022	0.851 \pm 0.031	0.884\pm0.016
BLCA	Accuracy (\uparrow)	0.952 \pm 0.005	0.952 \pm 0.005	0.955 \pm 0.000	0.968 \pm 0.011	0.966 \pm 0.014	0.970\pm0.006
	AUPRC (\uparrow)	0.652 \pm 0.106	0.688 \pm 0.098	0.617 \pm 0.086	0.686 \pm 0.114	0.653 \pm 0.085	0.724\pm0.101
	AUROC (\uparrow)	0.898 \pm 0.142	0.902 \pm 0.162	0.944 \pm 0.033	0.949 \pm 0.051	0.939 \pm 0.046	0.956\pm0.025
	MCC (\uparrow)	-0.005 \pm 0.009	-0.005 \pm 0.009	0.000 \pm 0.000	0.597 \pm 0.164	0.509 \pm 0.294	0.642\pm0.072
OV	Accuracy (\uparrow)	0.581 \pm 0.027	0.573 \pm 0.051	0.597 \pm 0.014	0.597 \pm 0.031	0.608 \pm 0.036	0.614\pm0.052
	AUPRC (\uparrow)	0.630 \pm 0.030	0.594 \pm 0.044	0.646\pm0.022	0.607 \pm 0.051	0.628 \pm 0.078	0.646\pm0.046
	AUROC (\uparrow)	0.621 \pm 0.037	0.603 \pm 0.062	0.655\pm0.025	0.630 \pm 0.040	0.652 \pm 0.067	0.652 \pm 0.056
	MCC (\uparrow)	0.199 \pm 0.071	0.126 \pm 0.138	0.201 \pm 0.029	0.199 \pm 0.060	0.225 \pm 0.073	0.228\pm0.104

trained for 200 epochs, with the batch size set to the total number of patients in each dataset due to the limited number of patients. All experiments are run on an Ubuntu 24.04 machine with an NVIDIA GeForce RTX 4090 GPU. More implementation details, including hyperparameter options and the selected configurations, are provided in the Supplementary Material (Appendix A). The source code of MAGNET is publicly available.²

5) *Baselines*: We compare MAGNET with five state-of-the-art multimodal fusion methods. MUSE [16] is a recent method that leverages bipartite graphs for direct prediction. MRGCN [47] uses an encoder-decoder framework based on GCNs for direct predictions with missing modalities. M3Care [15] is an imputation-based method that reconstructs missing modalities in the latent space by leveraging similarity between patients. MOGONET [10] is a supervised multiomics integration method based on GCN that requires complete modalities. To address missing modalities for MOGONET, we apply two imputation strategies, zero imputation and k -nearest neighbor (k NN), and refer to them as MOGONET-Zero and MOGONET- k NN. More details on these baselines are provided in the Supplementary Material (Appendix B).

B. Performance of Cancer Classification

Table III presents the classification performance of fusion methods on the BRCA, BLCA, and OV datasets. MAGNET consistently outperforms baseline multimodal fusion methods across all datasets and evaluation metrics, except for AUROC on OV, where it achieves the second-best result. Below, we provide detailed observations for each dataset.

1) *Results on BRCA*: MAGNET performs better than the best-performing direct prediction counterparts, MRGCN and MUSE, with improvements of 2.3% in accuracy, 2.2% in Macro F1, 2.3% in Weighted F1, and 3.88% in MCC. The weaker performance of MUSE may be due to overlapping feature distributions among certain BRCA classes, as it does not explicitly model direct patient-to-patient connections. Similarly, MRGCN fuses patient embeddings across modalities by assigning equal contributions, which may overlook the varying importance of different modalities. Moreover, both methods may struggle to handle severe modality missingness,

as their design assumptions might not effectively capture complex missing patterns. This limitation is further reflected in the performance of MOGONET-Zero, which shows the worst results across all metrics, suggesting that simple zero imputation is ineffective under such missingness.

2) *Results on BLCA*: MAGNET maintains its superior performance, achieving a 3.6% improvement in AUPRC and a 7.54% relative improvement in MCC over the best baseline, a particularly notable gain given the dataset’s class imbalance. In contrast, MOGONET with imputation yields the worst results across nearly all metrics for BLCA. This may be due to BLCA’s relatively low rate of missing modalities combined with a highly imbalanced class distribution, where even minor imputations can introduce errors that especially affect the already limited minority class.

3) *Results on OV*: On this well-balanced dataset, MAGNET demonstrates strong overall classification performance, achieving the highest accuracy, AUPRC, and MCC. However, its focus on correctly identifying the positive class may slightly affect ranking performance across all thresholds, leading to a marginally lower AUROC. Despite this, the overall results confirm the robustness of the method. Notably, while M3Care performs well on BRCA and BLCA, it ranks among the worst on OV, highlighting the difficulty for baselines to generalize across datasets with varying characteristics.

MAGNET’s superior results highlight the effectiveness of its PMMHA mechanism and graph-based modeling, enhancing multimodal fusion in the presence of missing modalities.

C. Analysis of Learned Representations

To further evaluate the effectiveness of MAGNET, we measure the separability of patient representations using two clustering metrics: Silhouette Score (SS) [59], where higher values indicate better-defined clusters, and Davies-Bouldin (DB) index [60], where lower values reflect better class separation. We extract the representations from the last layer of each trained model before generating predictions. Table IV presents the results on the test data for three datasets.

On **BRCA**, MAGNET improves SS and reduces DB, demonstrating its ability to separate classes effectively in a multiclass classification task. On **BLCA**, an imbalanced dataset, MAGNET achieves the lowest DB index, indicating strong global class

²<https://github.com/SinaTabakhi/MAGNET>

TABLE IV
SEPARABILITY EVALUATION OF PATIENT REPRESENTATIONS ON TEST DATA USING SILHOUETTE SCORE (SS) AND DAVIES-BOULDIN (DB) INDEX (BEST, SECOND-BEST).

Method	BRCA		BLCA		OV	
	SS (\uparrow)	DB (\downarrow)	SS (\uparrow)	DB (\downarrow)	SS (\uparrow)	DB (\downarrow)
MOGONET-Zero	0.214	1.447	0.836	0.741	0.024	4.491
MOGONET- k NN	0.354	1.078	0.870	0.757	0.034	4.395
MRGCN	0.145	1.658	0.261	0.700	0.006	8.808
M3Care	0.437	0.826	0.330	0.670	0.040	4.551
MUSE	0.408	0.879	0.295	0.793	0.047	3.900
MAGNET	0.440	0.789	0.578	0.642	0.048	4.433

separation. However, its SS is moderate, likely due to minority class patients being closer to decision boundaries. In contrast, imputation-based methods yield a higher SS by estimating missing values based on dominant patterns, which results in more compact clusters and improved local cohesion. On **OV**, a well-balanced dataset, MAGNET achieves the highest SS, highlighting well-clustered patient representations. However, its DB index remains average, likely because balanced class distributions result in uniform cluster compactness, reducing the inter-cluster contrast that DB emphasizes.

These results show MAGNET’s ability to enhance class separability across datasets while balancing local cohesion and global structure in learned representations.

D. Studies on Simulated Missing-Modality Scenarios

To further evaluate the impact of missing modalities, we use a publicly available simulated multiomics cancer dataset generated by the InterSim CRAN package, consisting of 500 samples across 15 clusters of varying sizes, reflecting realistic clinical scenarios. The dataset includes three omics modalities: DNA methylation, mRNA expression, and protein expression. The data is available on Zenodo [61], and further details about the data generation process can be found in the original publication [62].

To prepare the dataset for analysis, we normalize each feature to the [0, 1] range using min-max scaling, applied separately to each omics modality. The data is then split into training and test sets with a ratio of 8:2. We compare MAGNET with two top-performing baselines: M3Care and MUSE. For all methods, we use hyperparameters similar to those used for the BRCA dataset, given their comparable nature. We evaluate performance under several missing modality scenarios, and the results are presented in Fig. 3.

In the first scenario, we keep one omics modality intact while uniformly subsampling the other two at missingness ratios ranging from 0.2 to 0.8, with the zero-missingness case representing the complete dataset (Fig. 3(a)). The results show that MAGNET consistently outperforms the baselines across all missingness levels. Moreover, we observe that when DNA or protein modalities are kept intact, performance remains relatively stable, indicating that they are more informative. In contrast, when mRNA is the only intact modality, performance drops significantly, suggesting it is less predictive on its own.

In the second scenario, we retain a subset of patients that are shared across all three modalities and evenly assign the

remaining patients to individual modalities. The missingness ratio varies from 0.2 to 0.8 (Fig. 3(b)). We observe that MAGNET consistently achieves the highest performance across most settings. Notably, as the missingness ratio increases, the performance gap between MAGNET and the baseline methods also grows, highlighting the model’s robustness to missing modality information.

In the third scenario, we adopt a more complex setup where no omics modality is kept fully intact. Modalities are randomly masked with probabilities ranging from 0.2 to 0.8 (Fig. 3(c)). Performance results show that MAGNET consistently outperforms the baselines across all missingness levels. We also observe that as the masking probability increases, the performance gap between MAGNET and the baselines gets larger. For example, under severe missingness (80%), MAGNET improves performance by around 20% and 26% compared to M3Care and MUSE, respectively, demonstrating strong resilience to high levels of missing modalities. We also observe that M3Care, as an imputation-based method, experiences a much larger performance drop than the other methods as the missing probability increases. This may be because imputation-based methods rely on reconstructing missing data, which becomes increasingly difficult and error-prone as more information is missing.

E. Ablation Studies

We conduct ablation studies to evaluate the impact of individual components in MAGNET and assess its effectiveness.

1) *Classification Performance Analysis*: We evaluate the contribution of each component in MAGNET through seven modifications: (A1) removing the PMMHA mechanism and assigning equal contributions to modalities, (A2) removing the GNN architecture and applying the MLP decoder on the fused embedding, (A3) removing the edge feature from the patient interaction graph, (A4) removing the KL loss and using only the cross-entropy loss, and (A5)-(A7) replacing the GNN with a graph attention network (GAT) [63], graph convolutional network (GCN) [64], and graph isomorphism network (GIN) [65], respectively. Table V presents the results. We observe a significant performance drop when the PMMHA mechanism and GNN are removed, indicating that simple aggregation is insufficient for effective fusion in the presence of missing modalities, and that graph-based interactions are essential for capturing relational structure among patients. This is further supported by (A5)-(A7), where replacing the original GNN leads to a consistent drop, highlighting the suitability of GraphSAGE with the edge feature. Overall, these results validate the effectiveness of MAGNET.

2) *Learned Representation Analysis*: We evaluate eight types of representations used in the MAGNET architecture by measuring the separability of patient representations in the test data using SS and DB index: three input modalities, their learned representations from omics-specific encoders, the fused representation from PMMHA, and the final-layer representation produced by the GNN. Table VI presents the results, showing that in all cases across the three datasets, the final-layer representation learned by MAGNET achieves the

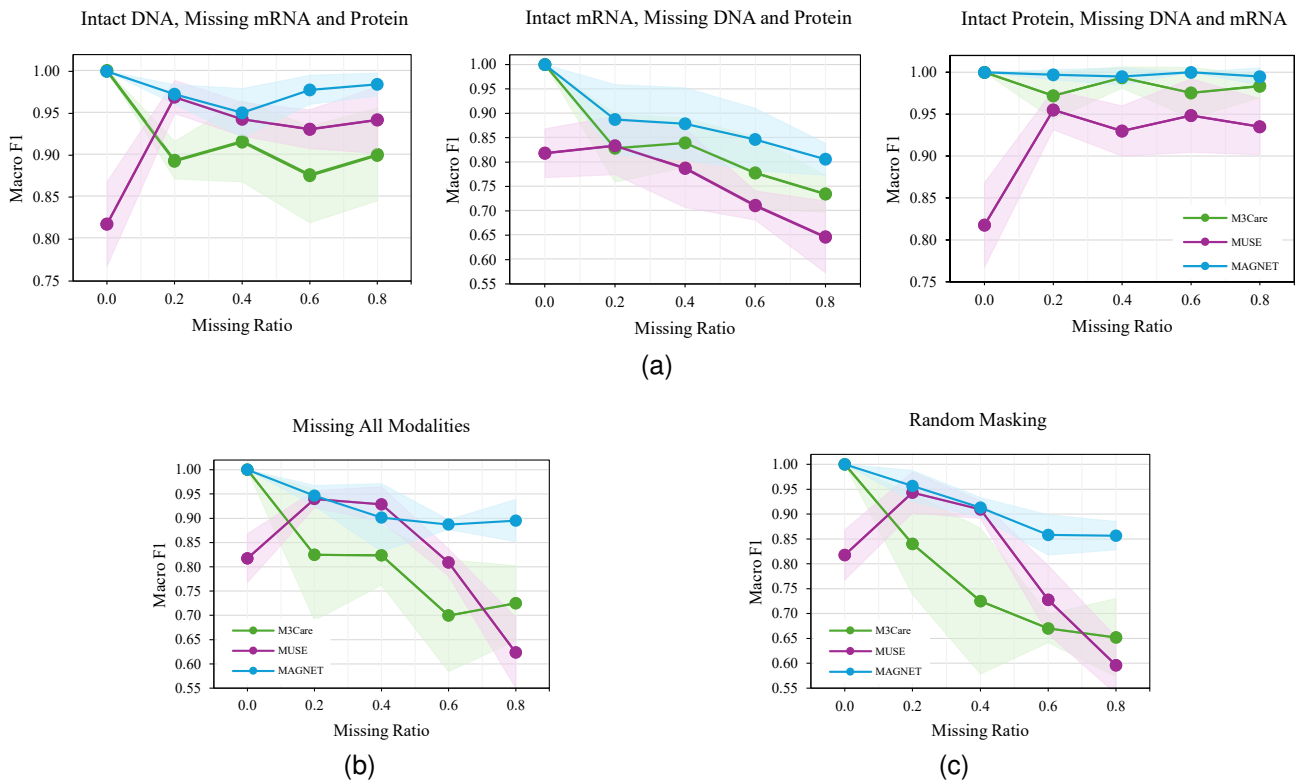


Fig. 3. Effect of varying missingness ratios on simulated cancer data using Macro F1, averaged over five independent runs per ratio. (a) One modality remains intact while the other two are uniformly subsampled. (b) A subset of patients is shared across all modalities, with the rest uniquely assigned to individual modalities. (c) Modalities are randomly masked with different probabilities.

TABLE V
ABLATION STUDY ON THE IMPACT OF EACH INDIVIDUAL COMPONENT OF MAGNET (BEST, SECOND-BEST).

ID	Method	BRCA	BLCA	OV
A1	MAGNET w/o PMMHA	0.905±0.016	0.681±0.064	0.600±0.049
A2	MAGNET w/o GNN	0.907±0.019	0.675±0.068	0.600±0.041
A3	MAGNET w/o Edge Feature	0.910±0.015	0.719±0.135	0.600±0.064
A4	MAGNET w/o KL Loss	0.911±0.013	0.686±0.104	0.592±0.071
A5	MAGNET w/ GAT	0.711±0.083	0.606±0.127	0.551±0.029
A6	MAGNET w/ GCN	0.823±0.002	0.609±0.110	0.567±0.041
A7	MAGNET w/ GIN	0.560±0.173	0.490±0.157	0.529±0.076
-	MAGNET	0.918±0.012	0.724±0.101	0.614±0.052

highest separability. Moreover, the representation learned from PMMHA alone achieves nearly the second-best result across all datasets compared to individual omics representations, suggesting that each added component in MAGNET contributes to producing more informative representations.

To further validate the effectiveness of fusing input omics modalities using MAGNET, we visualize the input omics modalities and the representations learned by the last layer of the GNN module in MAGNET. Fig. 4 shows the UMAP visualizations for the BRCA dataset, which contains a larger number of patients, providing better clarity compared to the other two datasets. We observe that among the individual omics modalities, mRNA demonstrates greater class separability on both the training and test data, whereas DNA and miRNA provide limited separability, with patients within the same classes overlapping significantly. Specifically, for the mRNA modality, while patients within the Normal-like and Basal-like

TABLE VI
SEPARABILITY EVALUATION OF PATIENT REPRESENTATIONS LEARNED FROM MAGNET MODULES ON TEST DATA USING SILHOUETTE SCORE (SS) AND DAVIES-BOULDIN (DB) INDEX (BEST, SECOND-BEST).

Module	BRCA		BLCA		OV	
	SS (↑)	DB (↓)	SS (↑)	DB (↓)	SS (↑)	DB (↓)
Input DNA	0.035	2.635	0.231	0.987	0.002	7.833
Input mRNA	0.105	2.276	0.120	1.531	0.006	5.264
Input miRNA	0.046	3.307	0.024	2.331	0.005	6.961
DNA Embedding	0.017	2.522	0.264	0.977	0.002	7.807
mRNA Embedding	0.246	1.170	0.188	1.284	0.018	4.618
miRNA Embedding	0.018	3.571	0.004	2.421	0.006	6.897
PMMHA Embedding	0.295	0.983	0.345	0.865	0.009	6.585
GNN Embedding	0.440	0.789	0.578	0.642	0.048	4.433

classes are relatively well separated, there is some overlap between patients in the Luminal A and Luminal B classes. In contrast, MAGNET effectively integrates these modalities, enhancing class separability. The fused representation not only distinguishes patients with similar classes more clearly but also achieves better separation between the Luminal A and Luminal B classes compared to the mRNA modality alone.

An ablation study on the importance of individual omics modalities and their combined integration is also provided in the Supplementary Material (Appendix C).

V. CONCLUSION

In this paper, we propose MAGNET, a novel method for direct prediction using partial omics modalities, without the need for imputation or patient exclusion, for cancer classification.

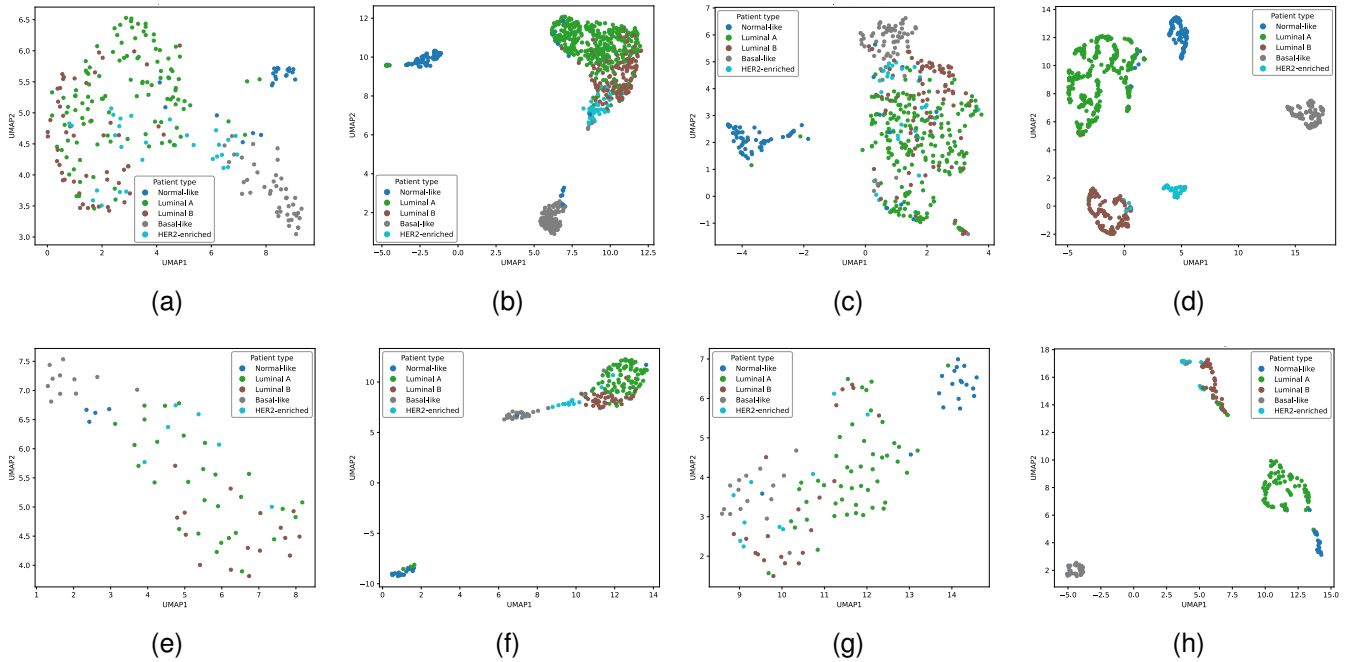


Fig. 4. UMAP visualization of the training and test data from the BRCA dataset across each input omics modality and the patient representations learned by the GNN module in MAGNET. (a)–(c) Training data from the input DNA, mRNA, and miRNA modalities, respectively. (d) Training data from the learned patient representations. (e)–(g) Test data from the input DNA, mRNA, and miRNA modalities, respectively. (h) Test data from the learned patient representations.

MAGNET introduces a patient-modality multi-head attention mechanism to fuse patient representations by learning the importance of each modality for a patient while adaptively masking out missing modalities. It also constructs a patient interaction graph using the input data with missing modalities for connectivity and the learned embeddings as node features. To preserve patient-level structure during fusion, MAGNET further incorporates a KL divergence-based loss that aligns similarity distributions before and after fusion. Key strengths of MAGNET include its linear complexity and extensibility with new modalities, as well as its robustness to diverse missing-modality patterns in both training and test data. Experimental results on three multiomics datasets with real-world missingness demonstrate its superiority over baseline methods. Furthermore, quantitative analysis of the learned representations validates its effectiveness.

This work focuses on biological datasets, specifically multiomics data for cancer classification, allowing targeted evaluation in a clinically relevant context. Future work will explore the integration of fundamentally different modalities, such as imaging and text, to support broader applicability. Although our experiments are limited to cancer-related applications, the proposed method is general and has the potential to be applied to non-biomedical domains.

REFERENCES

[1] C. Swanton, E. Bernard, C. Abbosh, F. André, J. Auwerx, A. Balmain, D. Bar-Sagi, R. Bernards, S. Bullman, J. DeGregori *et al.*, “Embracing cancer complexity: hallmarks of systemic disease,” *Cell*, vol. 187, no. 7, pp. 1589–1616, 2024.
 [2] C.-H. Yang, S.-H. Moi, L.-Y. Chuang, and Y.-D. Lin, “An information fusion system-driven deep neural networks with application to cancer mortality risk estimate,” *IEEE Transactions on Neural Networks and Learning Systems*, vol. 36, no. 2, pp. 2905–2916, 2025.

[3] X. Su, P. Hu, D. Li, B. Zhao, Z. Niu, T. Herget, P. S. Yu, and L. Hu, “Interpretable identification of cancer genes across biological networks via transformer-powered graph representation learning,” *Nature Biomedical Engineering*, pp. 1–19, 2025.
 [4] K. J. Karczewski and M. P. Snyder, “Integrative omics for health and disease,” *Nature Reviews Genetics*, vol. 19, no. 5, pp. 299–310, 2018.
 [5] J. N. Acosta, G. J. Falcone, P. Rajpurkar, and E. J. Topol, “Multimodal biomedical AI,” *Nature Medicine*, vol. 28, no. 9, pp. 1773–1784, 2022.
 [6] M. Zitnik, F. Nguyen, B. Wang, J. Leskovec, A. Goldenberg, and M. M. Hoffman, “Machine learning for integrating data in biology and medicine: principles, practice, and opportunities,” *Information Fusion*, vol. 50, pp. 71–91, 2019.
 [7] X.-A. Bi, W. Shen, Y. Shan, D. Chen, L. Xu, K. Chen, and Z. Liu, “MSAFF: multi-way soft attention fusion framework with the large foundation models for the diagnosis of Alzheimer’s disease,” *IEEE Transactions on Neural Networks and Learning Systems*, pp. 1–15, 2025.
 [8] L. Cantini, P. Zakeri, C. Hernandez, A. Naldi, D. Thieffry, E. Remy, and A. Baudot, “Benchmarking joint multi-omics dimensionality reduction approaches for the study of cancer,” *Nature Communications*, vol. 12, no. 1, p. 124, 2021.
 [9] B. Wang, A. M. Mezzini, F. Demir, M. Fiume, Z. Tu, M. Brudno, B. Haibe-Kains, and A. Goldenberg, “Similarity network fusion for aggregating data types on a genomic scale,” *Nature Methods*, vol. 11, no. 3, pp. 333–337, 2014.
 [10] T. Wang, W. Shao, Z. Huang, H. Tang, J. Zhang, Z. Ding, and K. Huang, “MOGONET integrates multi-omics data using graph convolutional networks allowing patient classification and biomarker identification,” *Nature Communications*, vol. 12, no. 1, p. 3445, 2021.
 [11] R. Mitra, S. F. McGough, T. Chakraborti, C. Holmes, R. Copping, N. Hagenbuch, S. Biedermann, J. Noonan, B. Lehmann, A. Shenvi *et al.*, “Learning from data with structured missingness,” *Nature Machine Intelligence*, vol. 5, no. 1, pp. 13–23, 2023.
 [12] M. Song, J. Greenbaum, J. Luttrell IV, W. Zhou, C. Wu, H. Shen, P. Gong, C. Zhang, and H.-W. Deng, “A review of integrative imputation for multi-omics datasets,” *Frontiers in Genetics*, vol. 11, p. 570255, 2020.
 [13] B. Vitrinel, H. W. Koh, F. M. Kar, S. Maity, J. Rendleman, H. Choi, and C. Vogel, “Exploiting interdata relationships in next-generation proteomics analysis,” *Molecular & Cellular Proteomics*, vol. 18, no. 8, pp. S5–S14, 2019.
 [14] Q. Wang, L. Zhan, P. Thompson, and J. Zhou, “Multimodal learning with incomplete modalities by knowledge distillation,” in *Proceedings*

- of the 26th ACM SIGKDD Conference on Knowledge Discovery & Data Mining, 2020, pp. 1828–1838.
- [15] C. Zhang, X. Chu, L. Ma, Y. Zhu, Y. Wang, J. Wang, and J. Zhao, “M3Care: learning with missing modalities in multimodal healthcare data,” in *Proceedings of the 28th ACM SIGKDD Conference on Knowledge Discovery and Data Mining*, 2022, pp. 2418–2428.
 - [16] Z. Wu, A. Dadu, N. Tustison, B. Avants, M. Nalls, J. Sun, and F. Faghri, “Multimodal patient representation learning with missing modalities and labels,” in *International Conference on Learning Representations*, 2024.
 - [17] M. Collier, A. Nazabal, and C. Williams, “VAEs in the presence of missing data,” in *ICML Workshop on the Art of Learning with Missing Values (Artemiss)*, 2020.
 - [18] J. Ngiam, A. Khosla, M. Kim, J. Nam, H. Lee, A. Y. Ng *et al.*, “Multimodal deep learning,” in *Proceedings of the 28th International Conference on Machine Learning*, vol. 11, 2011, pp. 689–696.
 - [19] W. Yao, K. Yin, W. K. Cheung, J. Liu, and J. Qin, “DrFuse: learning disentangled representation for clinical multi-modal fusion with missing modality and modal inconsistency,” in *Proceedings of the AAAI Conference on Artificial Intelligence*, vol. 38, 2024, pp. 16 416–16 424.
 - [20] J. You, X. Ma, Y. Ding, M. J. Kochenderfer, and J. Leskovec, “Handling missing data with graph representation learning,” *Advances in Neural Information Processing Systems*, vol. 33, pp. 19 075–19 087, 2020.
 - [21] M. Ma, J. Ren, L. Zhao, D. Testuggine, and X. Peng, “Are multi-modal transformers robust to missing modality?” in *Proceedings of the IEEE/CVF Conference on Computer Vision and Pattern Recognition*, 2022, pp. 18 177–18 186.
 - [22] N. Hayat, K. J. Geras, and F. E. Shamout, “MedFuse: multi-modal fusion with clinical time-series data and chest x-ray images,” in *Machine Learning for Healthcare Conference*. PMLR, 2022, pp. 479–503.
 - [23] Y.-H. H. Tsai, P. P. Liang, A. Zadeh, L.-P. Morency, and R. Salakhutdinov, “Learning factorized multimodal representations,” in *International Conference on Learning Representations*, 2019.
 - [24] M. Ma, J. Ren, L. Zhao, S. Tulyakov, C. Wu, and X. Peng, “SMIL: multimodal learning with severely missing modality,” in *Proceedings of the AAAI Conference on Artificial Intelligence*, vol. 35, 2021, pp. 2302–2310.
 - [25] M. K. Reza, A. Prater-Bennette, and M. S. Asif, “Robust multimodal learning with missing modalities via parameter-efficient adaptation,” *IEEE Transactions on Pattern Analysis and Machine Intelligence*, 2024.
 - [26] K. Lee, S. Lee, S. Hahn, H. Hyun, E. Choi, B. Ahn, and J. Lee, “Learning missing modal electronic health records with unified multi-modal data embedding and modality-aware attention,” in *Machine Learning for Healthcare Conference*. PMLR, 2023, pp. 423–442.
 - [27] R. M. Schouten, P. Lugtig, and G. Vink, “Generating missing values for simulation purposes: a multivariate amputation procedure,” *Journal of Statistical Computation and Simulation*, vol. 88, no. 15, pp. 2909–2930, 2018.
 - [28] Y. Zheng, Y. Liu, J. Yang, L. Dong, R. Zhang, S. Tian, Y. Yu, L. Ren, W. Hou, F. Zhu *et al.*, “Multi-omics data integration using ratio-based quantitative profiling with quartet reference materials,” *Nature Biotechnology*, vol. 42, no. 7, pp. 1133–1149, 2024.
 - [29] M. Kang, E. Ko, and T. B. Mersha, “A roadmap for multi-omics data integration using deep learning,” *Briefings in Bioinformatics*, vol. 23, no. 1, p. bbab454, 2022.
 - [30] S. Tabakhi, M. N. I. Suvon, P. Ahadian, and H. Lu, “Multimodal learning for multi-omics: a survey,” *World Scientific Annual Review of Artificial Intelligence*, vol. 1, p. 2250004, 2023.
 - [31] P. S. Reel, S. Reel, E. Pearson, E. Trucco, and E. Jefferson, “Using machine learning approaches for multi-omics data analysis: a review,” *Biotechnology Advances*, vol. 49, p. 107739, 2021.
 - [32] M. Chierici, N. Bussola, A. Marcolini, M. Francescato, A. Zandonà, L. Trastulla, C. Agostinelli, G. Jurman, and C. Furlanello, “Integrative network fusion: a multi-omics approach in molecular profiling,” *Frontiers in Oncology*, vol. 10, p. 1065, 2020.
 - [33] R. Schulte-Sasse, S. Budach, D. Hniz, and A. Marsico, “Integration of multiomics data with graph convolutional networks to identify new cancer genes and their associated molecular mechanisms,” *Nature Machine Intelligence*, vol. 3, no. 6, pp. 513–526, 2021.
 - [34] J. E. Flores, D. M. Claborn, Z. D. Weller, B.-J. M. Webb-Robertson, K. M. Waters, and L. M. Bramer, “Missing data in multi-omics integration: recent advances through artificial intelligence,” *Frontiers in Artificial Intelligence*, vol. 6, p. 1098308, 2023.
 - [35] B. Yang, Y. Yang, and X. Su, “Deep structure integrative representation of multi-omics data for cancer subtyping,” *Bioinformatics*, vol. 38, no. 13, pp. 3337–3342, 2022.
 - [36] Y. Pan, M. Liu, Y. Xia, and D. Shen, “Disease-image-specific learning for diagnosis-oriented neuroimage synthesis with incomplete modality data,” *IEEE Transactions on Pattern Analysis and Machine Intelligence*, vol. 44, no. 10, pp. 6839–6853, 2021.
 - [37] D. B. Rubin, “Multiple imputation after 18+ years,” *Journal of the American Statistical Association*, vol. 91, no. 434, pp. 473–489, 1996.
 - [38] J. L. Schafer, “Multiple imputation: a primer,” *Statistical Methods in Medical Research*, vol. 8, no. 1, pp. 3–15, 1999.
 - [39] P. C. Austin, I. R. White, D. S. Lee, and S. van Buuren, “Missing data in clinical research: a tutorial on multiple imputation,” *Canadian Journal of Cardiology*, vol. 37, no. 9, pp. 1322–1331, 2021.
 - [40] X. Dong, L. Lin, R. Zhang, Y. Zhao, D. C. Christiani, Y. Wei, and F. Chen, “TOBMI: trans-omics block missing data imputation using a k-nearest neighbor weighted approach,” *Bioinformatics*, vol. 35, no. 8, pp. 1278–1283, 2019.
 - [41] B. Gong, Y. Zhou, and E. Purdom, “Cobolt: integrative analysis of multimodal single-cell sequencing data,” *Genome Biology*, vol. 22, pp. 1–21, 2021.
 - [42] T. Ashuach, M. I. Gabitto, R. V. Koodli, G.-A. Saldi, M. I. Jordan, and N. Yosef, “MultiVI: deep generative model for the integration of multimodal data,” *Nature Methods*, vol. 20, no. 8, pp. 1222–1231, 2023.
 - [43] L. Cai, Z. Wang, H. Gao, D. Shen, and S. Ji, “Deep adversarial learning for multi-modality missing data completion,” in *Proceedings of the 24th ACM SIGKDD Conference on Knowledge Discovery & Data Mining*, 2018, pp. 1158–1166.
 - [44] C. Shang, A. Palmer, J. Sun, K.-S. Chen, J. Lu, and J. Bi, “VIGAN: missing view imputation with generative adversarial networks,” in *IEEE International Conference on Big Data*. IEEE, 2017, pp. 766–775.
 - [45] H. He, W. hao, Y. Xi, Y. Chen, B. Malin, and J. Ho, “A flexible generative model for heterogeneous tabular EHR with missing modality,” in *International Conference on Learning Representations*, 2024.
 - [46] N. Rappoport and R. Shamir, “NEMO: cancer subtyping by integration of partial multi-omic data,” *Bioinformatics*, vol. 35, no. 18, pp. 3348–3356, 2019.
 - [47] B. Yang, Y. Yang, M. Wang, and X. Su, “MRGCN: cancer subtyping with multi-reconstruction graph convolutional network using full and partial multi-omics dataset,” *Bioinformatics*, vol. 39, no. 6, p. btad353, 2023.
 - [48] J. Chen, S. Yang, X. Peng, D. Peng, and Z. Wang, “Augmented sparse representation for incomplete multiview clustering,” *IEEE Transactions on Neural Networks and Learning Systems*, vol. 35, no. 3, pp. 4058–4071, 2022.
 - [49] W. Hamilton, Z. Ying, and J. Leskovec, “Inductive representation learning on large graphs,” *Advances in Neural Information Processing Systems*, vol. 30, 2017.
 - [50] W. L. Hamilton, “Graph representation learning,” *Synthesis Lectures on Artificial Intelligence and Machine Learning*, vol. 14, no. 3, pp. 1–159, 2020.
 - [51] L. Van der Maaten and G. Hinton, “Visualizing data using t-SNE,” *Journal of Machine Learning Research*, vol. 9, no. 11, 2008.
 - [52] J. N. Weinstein, E. A. Collisson, G. B. Mills, K. R. Shaw, B. A. Ozenberger, K. Ellrott, I. Shmulevich, C. Sander, and J. M. Stuart, “The Cancer Genome Atlas Pan-Cancer analysis project,” *Nature Genetics*, vol. 45, no. 10, pp. 1113–1120, 2013.
 - [53] P.-K. Raj-Kumar, J. Liu, J. A. Hooke, A. J. Kovatich, L. Kvecher, C. D. Shriver, and H. Hu, “PCA-PAM50 improves consistency between breast cancer intrinsic and clinical subtyping reclassifying a subset of luminal A tumors as luminal B,” *Scientific Reports*, vol. 9, no. 1, p. 7956, 2019.
 - [54] The Cancer Genome Atlas Research Network, “Comprehensive molecular characterization of urothelial bladder carcinoma,” *Nature*, vol. 507, no. 7492, p. 315, 2014.
 - [55] Y. El-Manzalawy, T.-Y. Hsieh, M. Shivakumar, D. Kim, and V. Honavar, “Min-redundancy and max-relevance multi-view feature selection for predicting ovarian cancer survival using multi-omics data,” *BMC Medical Genomics*, vol. 11, no. 3, pp. 19–31, 2018.
 - [56] M. J. Goldman, B. Craft, M. Hastie, K. Repečka, F. McDade, A. Kamath, A. Banerjee, Y. Luo, D. Rogers, A. N. Brooks *et al.*, “Visualizing and interpreting cancer genomics data via the Xena platform,” *Nature Biotechnology*, vol. 38, no. 6, pp. 675–678, 2020.
 - [57] E. R. Girden, *ANOVA: repeated measures*. Sage, 1992, no. 84.
 - [58] D. P. Kingma and J. Ba, “Adam: a method for stochastic optimization,” in *International Conference on Learning Representations*, 2015.
 - [59] P. J. Rousseeuw, “Silhouettes: a graphical aid to the interpretation and validation of cluster analysis,” *Journal of Computational and Applied Mathematics*, vol. 20, pp. 53–65, 1987.

- [60] D. L. Davies and D. W. Bouldin, "A cluster separation measure," *IEEE Transactions on Pattern Analysis and Machine Intelligence*, vol. PAMI-1, no. 2, pp. 224–227, 1979.
- [61] S. Ma, "Dataset for "moving towards genome-wide data integration for patient stratification with integrate any omics";" Oct. 2024, Zenodo. [Online]. Available: <https://doi.org/10.5281/zenodo.13989262>
- [62] S. Ma, A. G. Zeng, B. Haibe-Kains, A. Goldenberg, J. E. Dick, and B. Wang, "Moving towards genome-wide data integration for patient stratification with integrate any omics," *Nature Machine Intelligence*, vol. 7, no. 1, pp. 29–42, 2025.
- [63] P. Veličković, G. Cucurull, A. Casanova, A. Romero, P. Liò, and Y. Bengio, "Graph attention networks," in *International Conference on Learning Representations*, 2018.
- [64] T. N. Kipf and M. Welling, "Semi-supervised classification with graph convolutional networks," in *International Conference on Learning Representations*, 2017.
- [65] K. Xu, W. Hu, J. Leskovec, and S. Jegelka, "How powerful are graph neural networks?" in *International Conference on Learning Representations*, 2019.
- [66] R. Liaw, E. Liang, R. Nishihara, P. Moritz, J. E. Gonzalez, and I. Stoica, "Tune: a research platform for distributed model selection and training," *arXiv preprint arXiv:1807.05118*, 2018.
- [67] L. Li, K. Jamieson, A. Rostamizadeh, E. Gonina, J. Ben-Tzur, M. Hardt, B. Recht, and A. Talwalkar, "A system for massively parallel hyperparameter tuning," *Proceedings of Machine Learning and Systems*, vol. 2, pp. 230–246, 2020.

Supplementary Material

APPENDIX

A. Hyperparameter Tuning

To ensure a fair comparison, we perform hyperparameter tuning for MAGNET and all baseline methods using the Ray Tune library [66]. We tune key hyperparameters that significantly influence model performance. For all methods, we run 100 trials with the Asynchronous Successive Halving Algorithm scheduler [67] to prioritize promising configurations. Each trial runs for up to 100 epochs, with training on the training set and evaluation on the validation set. To ensure robustness across data splits, we repeat each configuration five times and use the average performance for selection. Hyperparameter ranges are similar across methods unless otherwise specified in their original papers, in which case we adopt the recommended ranges. Table S7 lists the search spaces and the best-performing values for each dataset and method.

For MAGNET, we fix the number of layers in the MLP encoder, GNN, and MLP decoder to two across all datasets. The λ parameter is also set to 0.1.

TABLE S7
HYPERPARAMETER RANGES AND SELECTED VALUES ACROSS METHODS AND DATASETS.

Method	Hyperparameter	Range	BRCA	BLCA	OV
MAGNET	MLP Hidden Dimension	Grid Search ([128, 256])	128	256	256
	Patient Graph Sparsity Rate	Discrete Choice ([0.50-0.95], step 0.05)	0.60	0.60	0.80
	Dropout Rate	Discrete Choice ([0.0-0.3], step 0.1)	0.1	0.2	0.2
	#Heads in PMMHA	Grid Search ([2, 4, 8])	2	8	8
	Learning Rate	Log-Uniform (0.00001, 0.001)	0.00032	0.00017	0.000212
MOGONET-Zero	Hidden Dimension	Grid Search ([128, 256])	256	256	128
	#Edges Retained per Node	Integer Uniform ([2-10])	5	4	10
	Dropout Rate	Discrete Choice ([0.0-0.3], step 0.1)	0.3	0.3	0.1
	Pretraining Learning Rate	Log-Uniform (0.00001, 0.001)	0.00076	0.00014	0.000033
	Training Learning Rate	Log-Uniform (0.00001, 0.001)	0.00087	0.001	0.00074
MOGONET-kNN	Hidden Dimension	Grid Search ([128, 256])	128	256	128
	#Edges Retained per Node	Integer Uniform ([2-10])	2	2	2
	Dropout Rate	Discrete Choice ([0.0-0.3], step 0.1)	0.0	0.3	0.2
	Pretraining Learning Rate	Log-Uniform (0.00001, 0.001)	0.00095	0.00029	0.00021
	Training Learning Rate	Log-Uniform (0.00001, 0.001)	0.00083	0.00092	0.0008
MRGCN	#Neighbors per Node	Discrete Choice ([5, 10, 15, 20])	5	15	5
	Dropout Rate	Discrete Choice ([0.0-0.3], step 0.1)	0.2	0.0	0.0
	Learning Rate	Log-Uniform (0.00001, 0.001)	0.00023	0.000024	0.00011
M3Care	Hidden Dimension	Grid Search ([128, 256])	256	256	128
	Dropout Rate	Discrete Choice ([0.0-0.3], step 0.1)	0.2	0.3	0.1
	Learning Rate	Log-Uniform (0.00001, 0.001)	0.0002	0.00041	0.00019
MUSE	Hidden Dimension	Grid Search ([128, 256])	256	256	256
	Dropout Rate	Discrete Choice ([0.0-0.3], step 0.1)	0.3	0.1	0.3
	Learning Rate	Log-Uniform (0.00001, 0.001)	0.00072	0.00018	0.00035

B. Additional Details on Baselines

We compare the performance of MAGNET with the following state-of-the-art baseline fusion methods.

- **MUSE** [16] is a recently developed method for direct prediction in the presence of missing modalities in healthcare. This framework constructs a bipartite graph with modalities and patients as nodes, where the edge features represent the patient-specific features within each modality. From this initial graph, an additional graph is generated using edge dropout. These two bipartite graphs are then processed through a Siamese graph neural network to learn patient representations, which are used for final predictions through an MLP decoder.
- **MRGCN** [47] is a direct prediction method designed to handle missing modalities in multiomics data. It follows an encoder-decoder framework, where omics-specific encoders, based on GCN, generate representations that are simply aggregated to form a shared fusion across modalities. The decoder then reconstructs the input data structure. The method originally employs graph clustering on the fused data to further optimize the algorithm and facilitate downstream tasks. To ensure a fair comparison with MAGNET, we replace the clustering component with a two-layer MLP and use a cross-entropy loss function, similar to the architecture used in MAGNET.
- **M3Care** [15] is an imputation-based method for handling missing modalities in multimodal healthcare data. It first extracts latent representations from each input modality and computes patient similarities using learned deep kernels. These similarities are aggregated across available modalities to form a unified similarity matrix. Using this matrix, a patient graph is constructed for each modality by identifying similar patients, and a GNN is applied to learn patient

representations. Missing modalities are imputed in the embedding space based on these learned graphs. Finally, patient representations from all modalities are fused using a Transformer-based module for downstream tasks.

- **MOGONET [10]** is a supervised, late-fusion multiomics method. It employs omics-specific GCN to make initial predictions and then integrates label-level information from each omics modality using a view correlation discovery network to generate the final prediction. MOGONET assumes that all omics modalities are available for all patients. We consider MOGONET as a representative of this category and handle missing modalities using two imputation strategies: zero imputation and k NN imputation, referred to as **MOGONET-Zero** and **MOGONET- k NN**, respectively. For k NN-based imputation, we set $k = 10$ due to the limited number of patients in the multiomics datasets.

To ensure a fair comparison, all methods are trained for 200 epochs. For MOGONET, which includes both a pretraining and training phase, we allocate 100 epochs for pretraining and 100 epochs for training. All baselines are implemented using an inductive learning approach, where test sets are excluded during the training phase.

C. Importance of Individual Omics and Their Combined Integration

There are two key reasons for integrating multiple omics modalities. First, relying on a single modality limits prediction for patients missing that modality. For example, as shown in Table II, the BRCA dataset has approximately 66% missing DNA data. Using only DNA would exclude over half of the patients, highlighting the need to leverage other available modalities. Second, additional modalities can provide complementary information that enhances model performance beyond what a single modality can achieve. Although whether multiomics integration consistently improves performance remains an open question, our focus is on scenarios where integration offers improvements over single-modality models.

To explore this, we conduct an additional ablation study on the BRCA dataset. Specifically, we select patients who have data available for all three modalities, ensuring that when one or two modalities are removed, the remaining modalities are still present for every patient. We train MAGNET using seven different modality combinations: individual modalities, pairwise combinations of two modalities, and the full set of three modalities. When removing a modality, we mask it for the corresponding patients, treating it as a missing modality. The results of this experiment are shown in Fig. S5. The results show that although mRNA alone has the strongest predictive power among the three modalities, combining it with DNA further improves performance. Moreover, using all three modalities together yields the best overall results across all evaluation metrics.

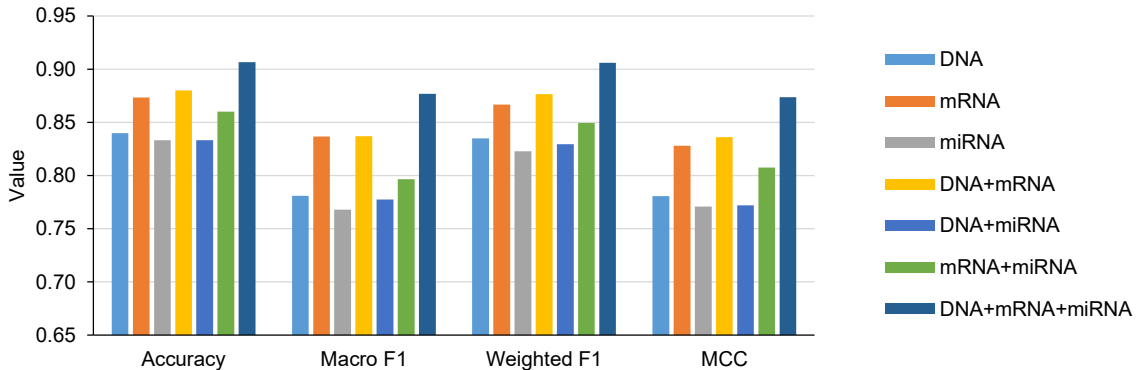


Fig. S5. Performance of MAGNET, averaged over five runs, across different combinations of omics modalities on the BRCA dataset.

D. Execution Time Analysis

We first evaluate the execution time versus classification performance of all methods during training on the BRCA, BLCA, and OV datasets. The results, averaged over five runs, are presented in Fig. S6. MAGNET achieves the best prediction performance among all methods, although its execution time is relatively higher than some baselines. This demonstrates that MAGNET offers a favorable trade-off between predictive performance and computational efficiency. Among the baselines, MAGNET execution time is slightly higher than that of the recent method MUSE. In contrast, M3Care as an imputation-based method shows the worst computational time which is almost double that of MAGNET. This highlights the high computational cost of imputation-based approaches. The lightweight computational time of MOGONET-Zero and MOGONET- k NN is attributed to the fact that their imputation is a simple procedure performed before training. However, this simplicity comes at the cost of significantly worse classification performance in almost all cases.

We next present the execution time of MAGNET with an increasing number of input modalities. To conduct this experiment, we retain only patients with all modalities available, ensuring that all modality combinations have the same number of patients, which allows a fair comparison. We report the average execution time over five runs for different combinations of modalities,

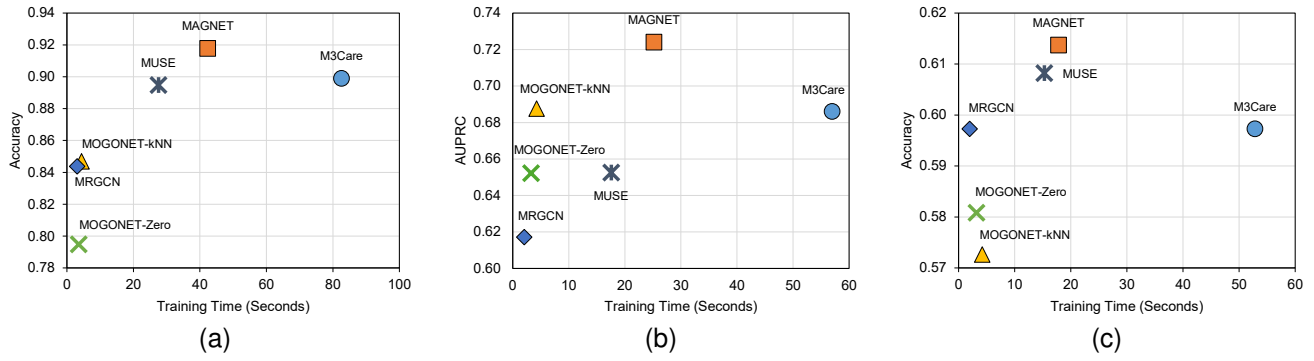


Fig. S6. Comparison of classification performance versus execution time, averaged over five runs. (a) BRCA results. (b) BLCA results. (c) OV results.

and the results are shown in Fig. S7. We observe that, across all datasets, the runtime increases approximately linearly as more modalities are added. This indicates that the computational cost of MAGNET scales linearly with the number of input modalities.

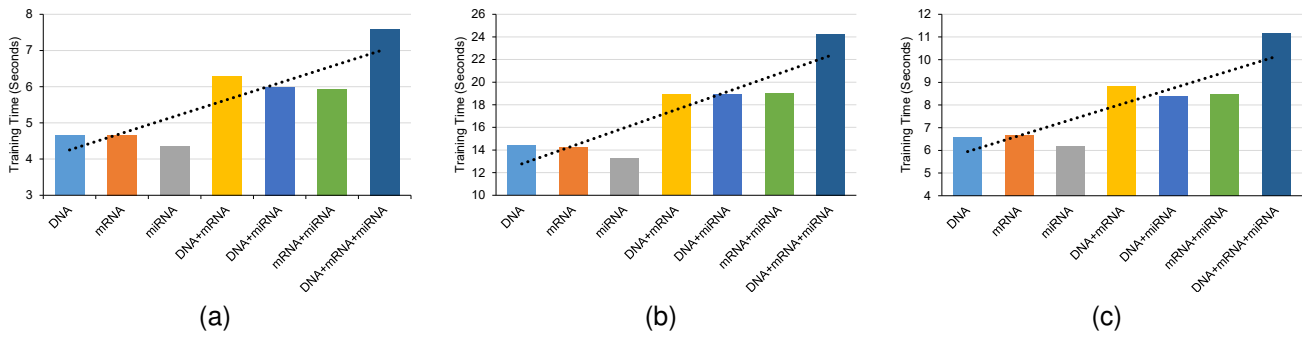


Fig. S7. Average execution time of MAGNET over five runs for different omics modality combinations. (a) BRCA results. (b) BLCA results. (c) OV results.